Novel self-powered ultraviolet photodetector with high photosensitivity based on Cu_2O/MgZnO heterojunction

YANHUA QU, YUE ZHU*, HAIYANG WANG
School of Automation, Shenyang Institute of Engineering, Shenyang 110136, China

Ultraviolet (UV) photodetectors (PDs) have garnered significant attention due to their extensive applications in civil and military fields. Self-powered photodetectors, which can operate without an external power supply, are anticipated to play a pivotal role in optoelectronic devices. The fabrication of heterojunction photodetectors can effectively utilize the built-in electric field formed by heterojunctions, thereby improving the performance of photodetectors. In this study, we design and construct a Cu_2O/MgZnO type-II heterojunction self-powered UV PD using a simple sol-gel process combined with the successive ionic layer adsorption and reaction (SILAR) method for the first time. The resulting self-powered UV PD demonstrates a remarkable responsivity of 35.48 mA/W, a detectivity of 1.1×10^{10} Jones, and a high photo-to-dark current ratio of 1283 under 325 nm illumination at zero bias. The built-in electric field generated by the type-II band alignment of the heterojunction facilitates the rapid separation of photogenerated carriers at the Cu_2O/MgZnO interface, thereby significantly enhancing the self-powered performance of the UV PD. Therefore, the UV PD constructed by Cu_2O/MgZnO type-II heterojunction shows a prominent self-powered performance. Furthermore, the photodetector presents a fast response speed with a rise time of 0.76 s and a decay time of 0.32 s. These performance metrics offer a cost-effective approach to improving photodetector properties, strongly suggesting that the Cu_2O/MgZnO UV PD holds great potential for high-performance, self-powered visible-blind photodetection.

(Received November 21, 2024; accepted June 3, 2025)

Keywords: Type-II heterostructure, Self-powered photodetector, Cu_2O, MgZnO

1. Introduction

Ultraviolet (UV) photodetectors (PDs) are widely used in various fields, such as flame sensing, pollution monitoring, optical communication, UV-emitter calibration, and astronomical exploration [1-5]. Typically, in order to obtain desirable photodetection results, most nanostructure-based UV PDs require an external power source to separate photogenerated carriers and generate a photocurrent. This not only greatly increases the size and energy consumption of the system but also greatly limits their long-term operation in some harsh environments and applications in areas such as in situ medical therapy monitoring and wireless environmental sensing. Therefore, developing self-powered systems that can operate independently, wirelessly, and sustainably is a significant research direction for next-generation nanodevices, offering a promising approach for UV PDs [6-8].

A novel self-powered UV PD that operates without an external power source is highly desirable for next-generation nanodevices due to its potential for reduced size, weight, and power consumption. One approach to achieving self-powered photoelectric detection is through the photovoltaic effect, which directly converts UV radiation into electrical energy [9-11]. For example, Liu et al. fabricated a self-powered deep-ultraviolet PD with a high detectivity of 5.94×10^{11} Jones at 0 V bias at 254 nm based on a CuI/Ga_2O_3 heterojunction [12]. Additionally, Das et al. reported a MgZnO-based self-powered UV PD with a very fast photoresponse of ~ 1.5 μs using a vertical Schottky junction in crossbar geometry [13]. Previous studies have demonstrated that p-n heterostructures significantly impact the multifunctionality and property tuning of self-powered UV PDs. Compared to other types, p-n heterojunctions can achieve enhanced light absorption and broader absorption ranges due to the presence of materials with different bandgaps, which significantly improves device performance and broadens the response spectrum. Thus, p-n junctions offer unique and substantially improved optical and optoelectronic properties through the combination of different functional components [14, 15].

Despite these advantages, there are still urgent issues to address for self-powered PDs based on p-n heterostructures, such as achieving high-quality and stable heterojunctions, which is crucial for realizing remarkable rectifying characteristics [16, 17]. $Mg_XZn_{1-X}O$, as a broadband gap n-type semiconductor, has attracted

widespread attention in the preparation of solar blind or visible blind UV PDs [18-22]. It not only has an adjustable band gap but also has strong radiation resistance and chemical stability [23-27], which has great potential among various applicable materials for fabricating high-performance UV PDs. However, the light current (I_l) and dark current (I_d) of MgZnO devices are limited by traps and low carrier mobility, hindering the realization of high responsivity (R) and detectivity (D^*) of the UV PD [2, 28-31].

The mechanism of the self-powered device can be understood n the energy band structure. Once in contact, a depletion region is formed at the n-type /p-type semiconductor materials interface due to carrier diffusion under thermal equilibrium conditions. This creates a built-in electric field that provides a driving force for charge separation. Therefore, the rational design of the p-n junction to enhance light absorption efficiency and improve interfacial charge dynamics is crucial for obtaining high photodetection performance [32, 33]. In this work, selecting the appropriate p-type material is a critical step in designing a self-powered UV PD based on MgZnO. A bandgap engineering device composed of the n-type MgZnO and a narrow bandgap p-type material is highly desirable for achieving a good response in the UV-Vis region. Cu_2O with a band gap of 2.17 eV is widely used in the field of photoelectric detection due to its simple and non-toxic synthesis method. Cu_2O, typically a p-type semiconductor due to Cu vacancies and excess oxygen, serves as an ideal candidate for constructing self-powered UV PDs [34-39]. When combined with n-type MgZnO, the Cu_2O/MgZnO p-n junction can effectively promote the separation of photoinduced carriers and broaden the range of light detection.

In this work, we reported a self-powered UV PD based on the Cu_2O/MgZnO p-n junction, constructed through a facile sol-gel process and a successive ionic layer adsorption and reaction (SILAR) method. The type-II heterojunction and the built-in electric field of p-Cu_2O/n-MgZnO favor an effective charge separation process and suppress carrier recombination that is desirable for excellent UV PD performance. The self-powered UV PD based on Cu_2O/MgZnO demonstrated significant rectifying behavior and a favorable self-powered phenomenon at zero bias. For example, it showed a high responsivity of 35.48 mA/W, a detectivity of 1.1×10^{10} Jones, and a fast response speed (rise time = 0.76 s, decay time = 0.32 s) under 325 nm light illumination. These excellent performances indicate that the Cu_2O/MgZnO device holds great promise for high-performance self-powered UV PD applications in the UV-Vis photo sensing field.

2. Experimental details

2.1. Preparation of Cu_2O/MgZnO heterojunction

The MgZnO film was prepared on the FTO substrate using the sol−gel method. MgZnO sol was synthesized by adding 1.77 g magnesium acetate tetrahydrate and 2.69 g zinc acetate dihydrate to 30 mL of isopropanol under continuous stirring at 75 ^oC for 30 min. Then, while maintaining a constant temperature of 75 ^oC, the amount of monoethanolamine equimolar to that of metal was added to get a homogeneously transparent solution. The solution was stirred for 2 h and finally left for 24 h at room temperature.

For the device manufacturing process, the FTO substrate was washed with acetone, ethanol, and deionized water for 15 min and then dried with N_2. Then, the MgZnO sol−gel was spin-coated onto pre-cleaned FTO substrates at 3000 rpm for 30 s, followed by heating at 180 °C for 10 min. The process was repeated six times to obtain the MgZnO film with a thickness of about 150 nm. After that, the samples were annealed at 500 ^oC for 2 h to form polycrystalline oxide thin films.

The Cu_2O film was deposited on the surface of MgZnO by the SILAR method. One SILAR cycle consisted of 3 steps: (1) adsorption of copper oxide species for 20 s by immerging the MgZnO substrate into the first anionic precursor solution ($Na_2S_2O_3$ and $CuSO_4$), (2) reaction with the first cationic precursor solution (NaOH) for another 20 s to form a stable Cu_2O layer by transferring the substrate to the second beaker, (3) rinsing with deionized water to remove excess or unreacted species or powdery Cu_2O.

2.2. Fabrication of heterojunction photodetector

The p-n heterojunction PDs were fabricated by the growth of a MgZnO layer on the FTO substrate followed by a Cu_2O layer. A total of three types of devices were prepared with different SILAR cycles of Cu_2O, the Cu_2O/MgZnO heterojunction prepared with 5, 10, and 15 cycles was marked as Cu_2O/MgZnO (5), Cu_2O/MgZnO (10), and Cu_2O/MgZnO (15), respectively. Finally, a layer of 100 nm thick gold was evaporated as an electrode.

2.3. Characterization of the materials and the devices

The surface morphology was analyzed by a Bruker Dimension Icon atomic force microscope (AFM). X-ray diffraction (XRD) measurement was performed by using a Shimadzu XRD-6000 diffractometer. A Shimadzu UV-1700 Pharma Spec UV spectrophotometer was used to obtain the UV-Vis absorption spectrum. X-ray photoelectron spectroscopy (XPS) measurements were performed using an ESCALAB 250 spectrometer. Use Keithley 2601 digital source meter for current-voltage (I-V) measurement. A 30 W deuterium lamp is used as the light source, and the monochromatic light is provided by the monochromator.

3. Results and discussion

Figs. 1a and 1b illustrate the surface morphology of the MgZnO film and the Cu_2O/MgZnO composite film as measured by AFM measurement. In this work, 10 SILAR cycles were applied to form Cu_2O, with the thickness of the Cu_2O layer being approximately 120 nm [40]. Both films exhibit smooth and compact surface morphologies, indicating their potential for excellent light absorption and charge transport capacities. After ten SILAR cycles of depositing Cu_2O, the root-mean-square roughness (*R*q) increases from 7.30 nm to 9.28 nm. This increase in roughness indicates that the Cu_2O film is slightly rougher than the underlying MgZnO film. The observed surface roughness is beneficial as it can enhance light scattering and absorption, thereby improving the overall performance of the PD.

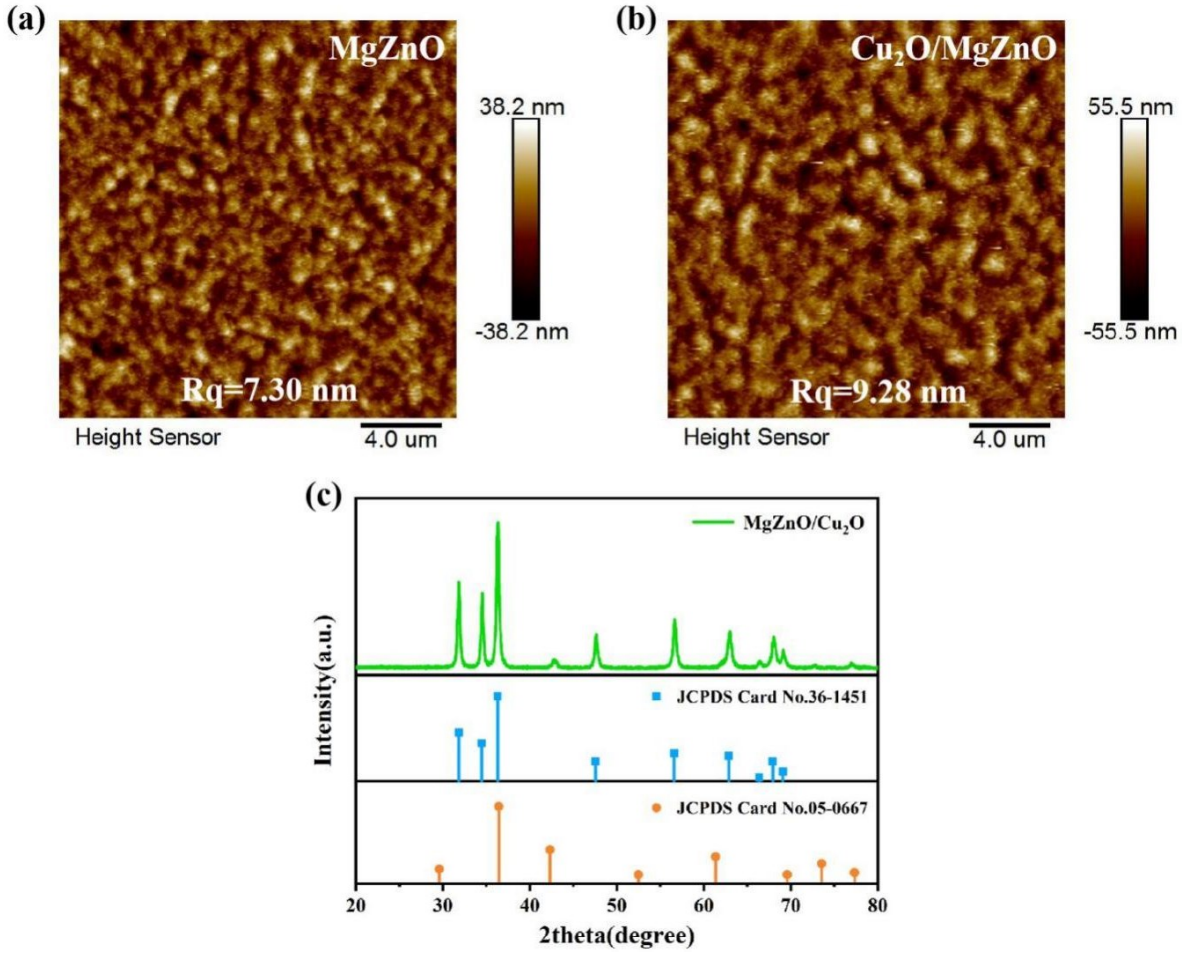

Fig. 1. AFM images of (a) pristine MgZnO film and (b) Cu_2O/MgZnO composite film. (c) XRD pattern of MgZnO/Cu_2O composite film (colour online)

The XRD spectra of the Cu_2O/MgZnO heterojunction are shown in Fig. 1c. It was noticed that only one diffraction peak is observed at $2\theta = 34.75^{\circ}$, which corresponds to the (002) orientation of the MgZnO hexagonal structure [2]. For the double-layer membrane structure, the hexagonal phase crystal structure of Mg-doped ZnO remains intact because the concentration of Mg-doped ZnO is only 20%. However, no peaks corresponding to Cu_2O are detected, indicating that the Cu_2O film is amorphous. This absence of crystalline peaks for Cu_2O suggests that the film is not crystallized under the given experimental conditions, which might be due to the low-temperature process used for its deposition. The XPS results for the Cu 2p ionizations of the Cu_2O composites are shown in Fig. 2a.

The typical two-peak structure (Cu 2p3/2 at 932.8 eV and Cu 2p1/2 at 952.8 eV) due to the spin-orbit splitting is observed for the Cu 2p signal, confirming the initial (+I) state of copper in the composite [41]. The satellite peak located at 938.0 - 947.0 eV corresponds to Cu^{2+}, which is primarily due to the unavoidable oxidation of a small amount of Cu_2O on the surface when exposed to air [42, 43]. The O 1s core level spectra of MgZnO, as shown in Fig. 2b, can be deconvoluted into a lower binding energy peak at 530.4 eV attributed to the lattice oxygen in MgZnO and a higher binding energy peak at 531.9 eV associated with the chemisorbed oxygen caused by surface hydroxyl, respectively [44, 45]. Compared with the pristine MgZnO sample, the peak area of lattice oxygen decreases sharply due to the formation of the Cu_2O layer,

as shown in Fig. 2c. In addition, the O 1s peaks corresponding to MgZnO and OH groups shift to higher energy. This shift can be ascribed to the strong interaction between MgZnO and Cu_2O. These structural characterization results demonstrate the successful synthesis of the Cu_2O/MgZnO heterojunction with the desired chemical states and interfacial properties, which are crucial for the enhanced performance of the self-powered ultraviolet photodetector.

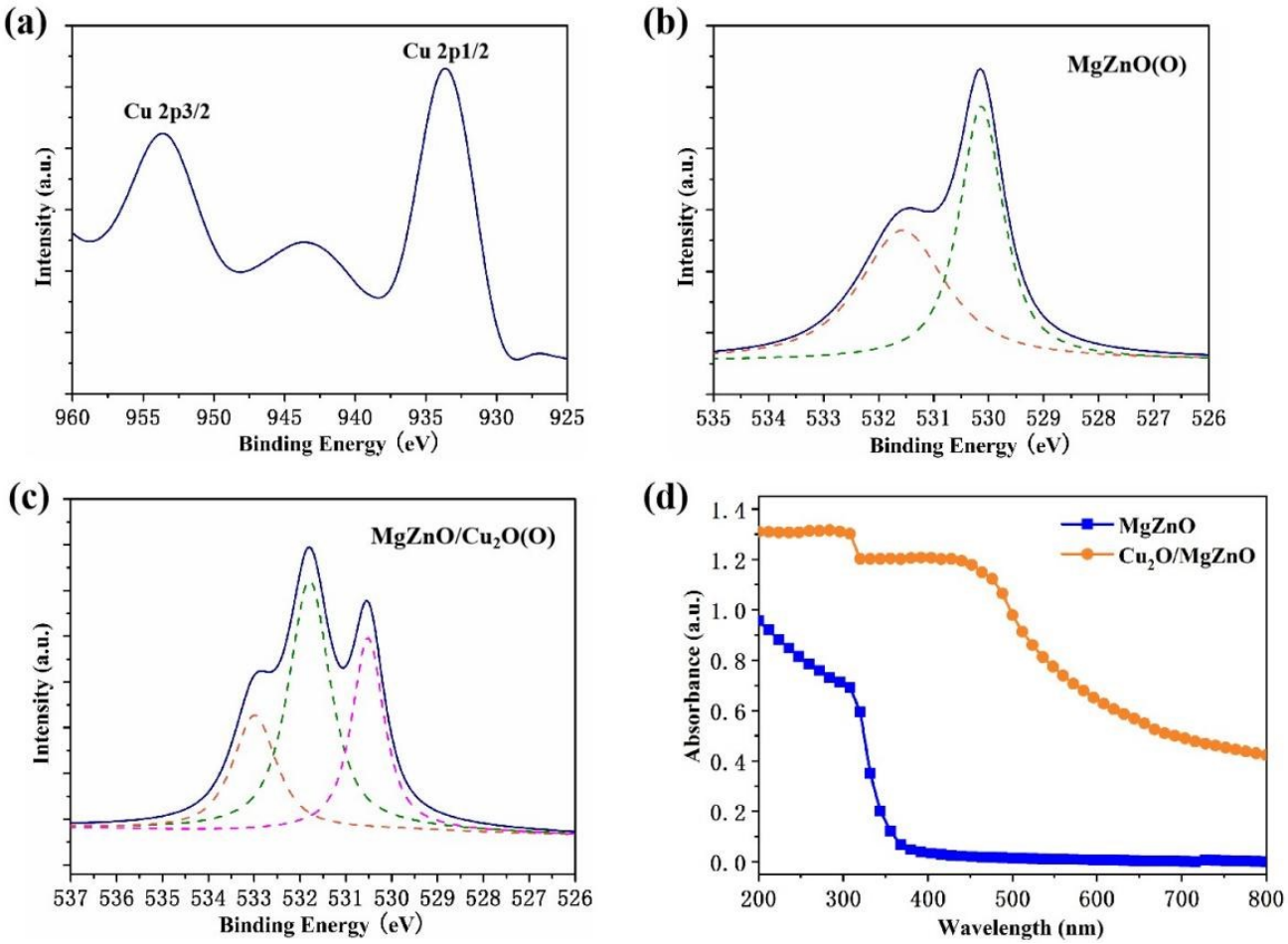

Fig. 2. (a) Cu 2p of MgZnO/Cu_2O composite film. XPS high-resolution survey scan of (b) O 1s of MgZnO pristine film and (c) O 1s of MgZnO/Cu_2O composite film. (d) Absorbance spectra of pristine MgZnO and MgZnO/Cu_2O composite film (colour online)

Fig. 2d displays the absorption spectra of the MgZnO film and Cu_2O/MgZnO heterojunction films in the range of 200 - 800 nm. After the deposition of Cu_2O films, absorption has been obviously enhanced in the UV-Vis region. This can be attributed to the good absorption characteristics of Cu_2O films, which will improve the light-harvesting of the composite film and result in higher photodetector performance. Fig. 3a presents a schematic of the self-powered heterojunction PD based on the Cu_2O/MgZnO. In order to create a sandwich structure, the Cu_2O/MgZnO composite film is clamped between the FTO substrate and Au electrode. This device configuration effectively promotes carrier separation by shortening the migration length of the carriers compared to the traditional interdigital structure. The compact sandwich design enhances the efficiency of the photogenerated carrier collection, thereby improving the overall performance of the photodetector. This innovative structure not only ensures efficient charge transport but also contributes to the device's high photosensitivity and self-powered operation.

Fig. 3b shows the current−voltage (I-V) characteristics of Cu_2O/MgZnO (5), Cu_2O/MgZnO (10), and Cu_2O/MgZnO (15) under dark conditions and 325 nm UV illumination, with a bias range from −1 to 1 V. We can find that the heterojunction devices exhibit resistance characteristics in the dark state and generate a zero-bias photocurrent under UV irradiation. The nonsymmetrical I–V curves show an obvious open-circuit voltage (V_{oc}) and short-circuit current (I_s) when exposed to UV light, indicating that the heterojunction device has a photovoltaic effect under UV light illumination, enabling self-powered UV light detection. This can be attributed to the high-quality interface between Cu_2O and MgZnO. As the thickness of the Cu_2O film increases, the photocurrent under UV light for Cu_2O/MgZnO heterojunction devices initially increases and then decreases without an externally applied bias. This is mainly related to the film thickness, light absorption process, and defects [46]. The photocurrent reaches its maximum value for the

Cu_2O/MgZnO (10) device. Additionally, the Cu_2O/MgZnO (10) device exhibits a relatively larger V_{oc} of 0.27 V, I_s of 1.6×10^{-6} A, and a photo-to-dark current ratio of 1283 at zero bias. Generally, the V_{oc} is related to the built-in electric field of the heterojunction. This phenomenon can be understood through the built-in electric field at the Cu_2O and MgZnO film interface, which provides a barrier that reduces the dark current. Meanwhile, the built-in electric field acts as a driving force to separate electron-hole pairs under light illumination, thereby realizing a self-powered system. This efficient charge separation and reduced recombination contribute to the superior performance of the Cu_2O/MgZnO heterojunction photodetector.

Fig. 3c shows the photoresponsivity (R) under light illumination from 250 to 400 nm under zero bias. The $R(\lambda)$ could be calculated according to the following equation:

$$\boldsymbol{R(\lambda) = \frac{I_l(\lambda)}{P(\lambda) \times A}} \quad (1)$$

where $I_l(\lambda)$ is the measured I_l of the device under zero bias at different wavelengths, $P(\lambda)$ is the corresponding incident light intensity, and A is the effective area of the device. The maximum R of the Cu_2O/MgZnO (10) device is 35.48 mA/W at 0 V bias. Detectivity (D^*) is also the essential parameter to evaluate the performance of the PDs. The D^* reflects the ability of a photodetector to detect the weakest detectable signals from the noise environment. Due to the dominant contribution of dark current, we expected to reduce noise by decreasing the level of dark current. It can be calculated using the following equation [47]:

$$\boldsymbol{D^* = \frac{R(\lambda)}{(2eI_d/A)^{1/2}}} \quad (2)$$

where e refers to the electronic charge. Due to the suppressed dark current and enhanced responsivity, the D^* of the Cu_2O/MgZnO device has a maximum value of 1.1×10^{10} Jones. So, the above experimental data reveals that Cu_2O/MgZnO photodetector has excellent self-powered performances.

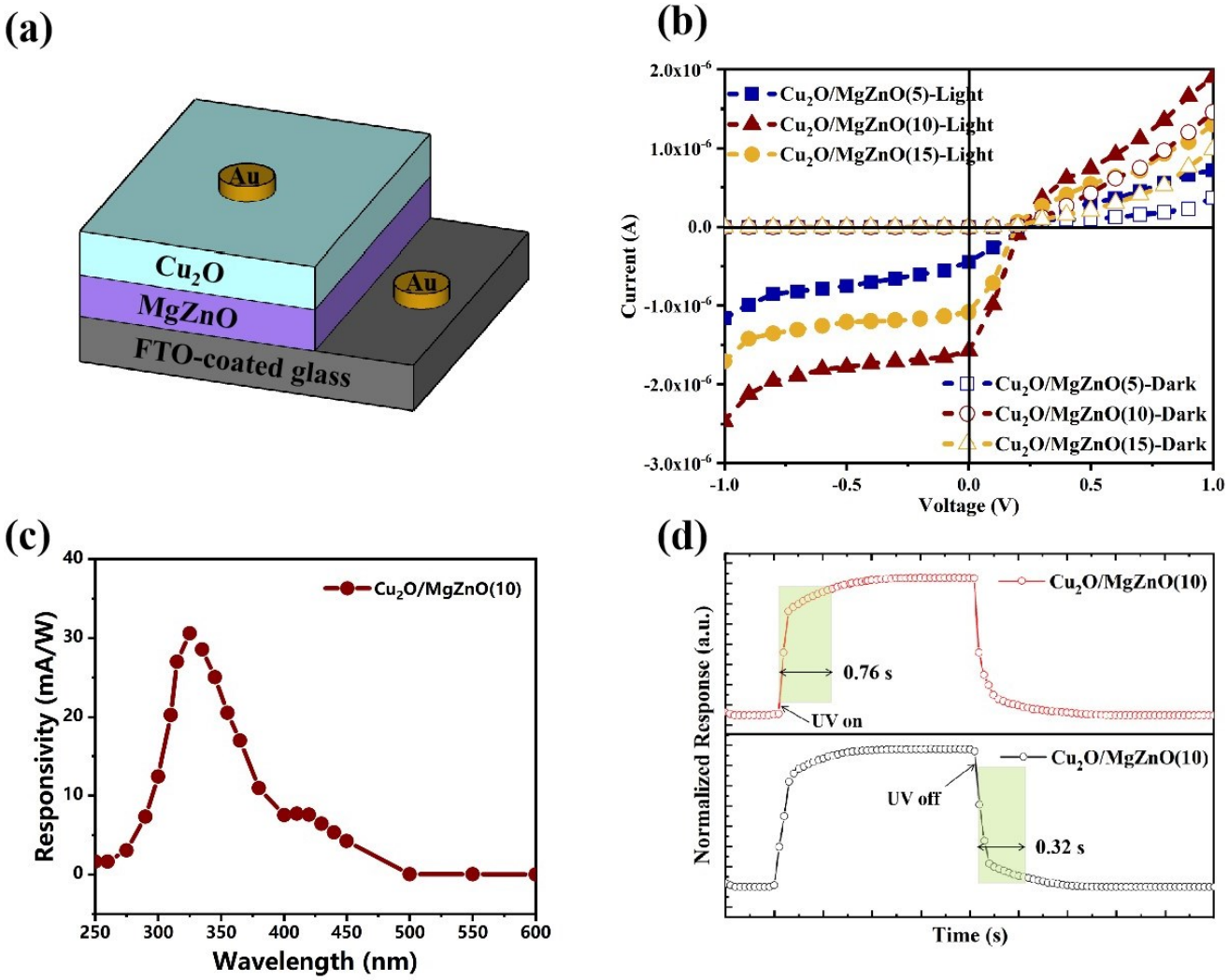

Fig. 3. (a) Structure of the Cu_2O/MgZnO heterojunction UV PD. (b) I-V characteristics of all devices under UV illumination and in the dark. Spectral R (c) and time response characteristics (d) of the Cu_2O/MgZnO-10 device (colour online)

The response time of the Cu_2O/MgZnO device under zero bias was measured using a rapid photoresponse measurement system, as shown in Fig. 3d. The rise time (from 10% to 90% of the top value) and the decay time (from 90% to 10% of the top value) were calculated to be 0.76 and 0.32 s for the Cu_2O/MgZnO device at zero bias, respectively. When transitioning from UV off to on, the photo-induced electron and hole pairs are quickly separated by the built-in electric field within the depletion region of the Cu_2O/MgZnO heterojunction. Conversely, when transitioning from UV on to off, the phenomenon of sustainable photoconductivity is avoided due to the effective charge separation and recombination processes facilitated by the Cu_2O/MgZnO heterojunction. This indicates that the device exhibits a fast and reliable photoresponse, making it highly suitable for applications requiring rapid UV detection.

The exceptional self-powered performance of the Cu_2O/MgZnO heterojunction UV PD is attributed to the heterojunction interface contact and carrier transmission characteristics, which function efficiently without the need for an externally applied bias. Cu_2O effectively passivates the surface of MgZnO, mitigating shallow defects such as surface oxygen vacancies. Moreover, the Cu_2O/MgZnO heterojunction demonstrates significantly enhanced UV-light absorption due to the synergistic integration of the two materials. To gain a comprehensive understanding of the mechanism behind the self-powered Cu_2O/MgZnO device, we explored its energy band structure. It is well-established that the performance of a heterojunction is heavily influenced by the band alignments at the contact interface. The energy alignment levels of the Cu_2O/MgZnO heterojunction are depicted in Fig. 4, indicating a type-II band alignment at the Cu_2O/MgZnO interface [48-51]. The band gap values of Cu_2O and MgZnO are 2.17 and 3.46 eV, respectively. The electron affinities of Cu_2O and MgZnO are 3.3 and 4.28 eV, respectively. The valence band offset (ΔE_V) and the conduction band offset (ΔE_C) of the Cu_2O/MgZnO heterojunction are 2.27 and 0.98 eV [52-55]. The traditional type-II heterostructure is an effective strategy for enhancing photodetector performance, as it facilitates charge transport and the rapid separation of photo-generated electron-hole pairs [56, 57]. The depletion region at the contact interface of p-type Cu_2O and n-type MgZnO is formed due to the difference in their Fermi energy levels. In the dark state, the depleted heterojunction effectively reduces the majority carrier concentration, resulting in a high resistance state for the Cu_2O/MgZnO heterojunction and thereby reducing the dark current of the device. Simultaneously, a substantial built-in electric field in the depletion region, directed from MgZnO towards Cu_2O, provides a robust driving force for the separation and transmission of photogenerated carriers. Upon UV light illumination, the built-in electric field separates the photo-generated electron-hole pairs within the depletion region. The separated carriers are transported to the electrodes without the need for an external bias, leading to the device's remarkable self-powered performance [58-63]. This performance is attributed to the well-aligned band structures of FTO, MgZnO, Cu_2O, and Au, whose electron affinities and Fermi levels are closely coordinated.

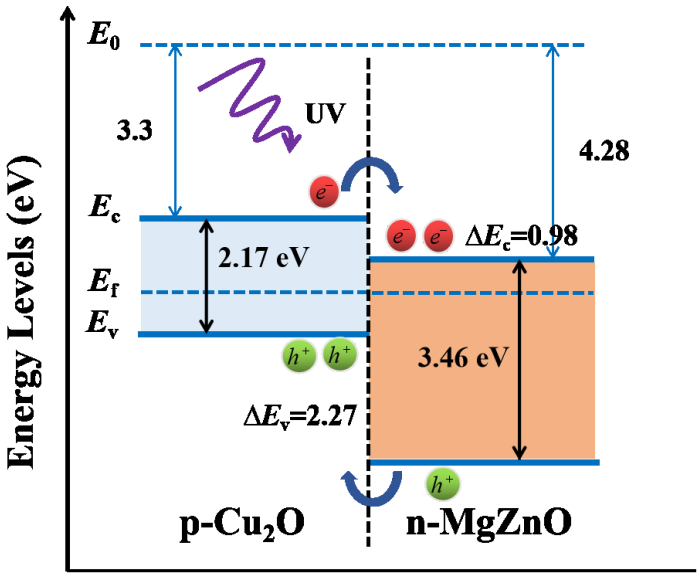

Fig. 4. The energy level diagrams between Cu_2O and MgZnO (colour online)

4. Conclusion

In summary, we successfully prepared Cu_2O films using the SILAR method and fabricated a Cu_2O/MgZnO heterojunction UV PD with outstanding self-powered performance. The excellent performance of this device is attributed to its excellent heterojunction interface contact and carrier transport characteristics. The Cu_2O/MgZnO PD exhibits a large photo-to-dark current ratio of 1283, a responsivity of 35.48 mA/W, and a detectivity of 1.1×10^{10} Jones, all achieved without an external bias. Additionally, the device demonstrates a fast response time, with a rise time of 0.76 s and a decay time of 0.32 s. The formation of a type-II heterostructure facilitates the efficient distribution of electrons and holes in Cu_2O and MgZnO. These exceptional performances indicate that the Cu_2O/MgZnO device holds significant potential and is an excellent candidate for high-performance self-powered UV photodetectors.

Acknowledgments

The authors are grateful to the Project of Applied Basic Research Plan of Liaoning Province (Grant No. 2023JH2/101300180) for the support of this work.

References

[1] S. Cai, C. Zuo, J. Zhang, H. Liu, X. Fang, Advanced Functional Materials **31**(20), 2100026 (2021).
[2] Y. Duan, S. Zhang, M. Cong, D. Jiang, Q. Liang, X. Zhao, Journal of Materials Chemistry C **8**(37), 12917 (2020).
[3] S. K. Kajli, D. Ray, S. C. Roy, Journal of Alloys and Compounds **895**, 162546 (2022).
[4] M. Kumar, J. Y. Park, H. Seo, Advanced Optical Materials **10**(10), 2102532 (2022).
[5] H. T. D. S. Madusanka, H. M. A. M. C. Herath, C. A. N. Fernando, Sensors and Actuators A: Physical **296**, 61 (2019).
[6] X. Zhang, Z. Li, E. Hong, T. Yan, X. Fang, Advanced Materials **37**(3), 2412014 (2025).
[7] D. Nematov, Journal of Optics and Photonics Research **1**(2), 91 (2024).
[8] X. Zhang, Z. Li, T. Yan, L. Su, X. Fang, Small **19**(9), 2206310 (2023).
[9] H. Lin, L. Wei, C. Wu, Y. Chen, S. Yan, L. Mei, J. Jiao, Nanoscale Research Letters **11**, 1 (2016).
[10] Y. Lin, J. Zou, W. Wang, X. Liu, J. Gao, Z. Lu, Applied Surface Science **599**, 153956 (2022).
[11] T. Ouyang, X. Zhao, X. Xun, F. Gao, B. Zhao, S. Bi, Qi Li, Qingliang Liao, Y. Zhang, Advanced Science **10**(23), 2301585 (2023).
[12] Y. Liu, L. Shen, X. Pan, T. Zhang, H. Wu, N. Wang, P. Wang, F. Wang, Z. Ye, Sensors and Actuators A: Physical **349**, 114068 (2023).
[13] A. K. Das, V. K. Sahu, R. S. Ajimsha, P. Misra, Sensors and Actuators A: Physical **362**, 114612 (2023).
[14] Y. Peng, J. Lu, X. Wang, W. Ma, M. Que, Q. Chen, Fangtao Li, Xianhu Liu, Wenchao Gao, C. Pan, Nano Energy **94**, 106945 (2022).
[15] Q. Zhang, J. Xu, M. Li, J. Chen, J. Xu, Q. Zheng, S. Shi, L. Kong, X. S. Zhang, L. Li, Applied Surface Science **592**, 153350 (2022).
[16] S. Li, Z. Chen, Z. Du, H. He, X. Shen, Y. Fu, Optics Communications **525**, 128838 (2022).
[17] C. Zuo, S. Cai, Z. Li, X. Fang, Nanotechnology **33**(10), 105202 (2021).
[18] H. Chen, P. Yu, Z. Zhang, F. Teng, L. Zheng, K. Hu, X. Fang, Small **12**(42), 5809 (2016).
[19] S. Han, S. M. Liu, Y. M. Lu, P. J. Cao, W. J. Liu, Y. X. Zeng, F. Jia, X. K. Liu, D. L. Zhu, Journal of Alloys and Compounds **694**, 168 (2017).
[20] R. Kara, L. Mentar, A. Azizi, RSC Advances **10**(66), 40467 (2020).
[21] Y. Li, R. Deng, B. Yao, G. Xing, D. Wang, T. Wu, Applied Physics Letters **97**(10), 102506-3 (2010).
[22] H. Wang, Q. Liu, X. Ma, H. Liu, X. Zhang, Journal of Materials Science: Materials in Electronics **29**, 13052 (2018).
[23] B. Amrani, R. Ahmed, F. E. H. Hassan, Computational Materials Science **40**(1), 66 (2007).
[24] K. Gu, X. Zhou, Z. Zhang, K. Tang, J. Huang, L. Wang, Materials Letters **278**, 128416 (2020).
[25] Y. J. Shi, R. J. Zhang, X. Chen, L. Wang, L. Chen, Q. H. Huang, D. H. Li, Y. X. Zheng, S. Y. Wang, N. Dai, L. Y. Chen, Physical Chemistry Chemical Physics **20**(39), 25467 (2018).
[26] M. Xue, Q. Guo, K. Wu, J. Guo, The Journal of Chemical Physics **129**(23), 234707 (2008).
[27] S. K. Kang, M. Kim, G. H. Park, J. Ji, S. Hong, W. B. Kim, Advanced Functional Materials **35**(2), 2408986 (2025).
[28] Y. N. Hou, Z. X. Mei, H. L. Liang, D. Q. Ye, S. Liang, C. Z. Gu, X. L. Du, Applied Physics Letters **98**(26), 263501 (2011).
[29] H. Wang, A. Wang, Y. Sun, L. Wu, W. Wang, J. Zhang, L. Feng, Applied Surface Science **503**, 144273 (2020).
[30] S. Shahzad, S. Javed, M. Usman, Frontiers in Materials **8**, 613825 (2021).
[31] R. Ghosh, D. Basak, Journal of Applied Physics, **101**(11), 113111 (2007).
[32] S. M. Hatch, J. Briscoe, S. Dunn, Advanced Materials **25**(6), 867 (2012).
[33] L. Zheng, F. Teng, Z. Zhang, B. Zhao, X. Fang, Journal of Materials Chemistry C **4**(42), 10032

(2016).
[34] Z. Bai, J. Liu, F. Liu, Y. Zhang, Journal of Alloys and Compounds **726**, 803 (2017).
[35] Z. Bai, Y. Zhang, Journal of Alloys and Compounds **675**, 325 (2016).
[36] L. Cong, H. Zhou, M. Chen, H. Wang, H. Chen, J. Ma, S. Yan, B. Li, H. Xu, Y. Liu, Journal of Materials Chemistry C **9**(8), 2806 (2021).
[37] P. Ghamgosar, F. Rigoni, S. You, I. Dobryden, M. G. Kohan, A. L. Pellegrino, I. Concina, N. Almqvist, G. Malandrino, A. Vomiero, Nano Energy **1**, 308 (2018).
[38] C. He, D. Guo, K. Chen, S. Wang, J. Shen, N. Zhao, A. Liu, Y. Zheng, P. Li, Z. Wu, C. Li, F. Wu, W. Tang, ACS Applied Nano Materials **2**(7), 4095 (2019).
[39] C. Y. Huang, X. R. He, ACS Applied Electronic Materials **4**(3), 1335 (2022).
[40] D. Ozaslan, O. M. Ozkendir, M. Gunes, Y. Ufuktepe, C. Gumus, Optik **157**, 1325 (2018).
[41] J. Khanderi, C. Contiu, J. Engstler, R. C. Hoffmann, J. J. Schneider, A. Drochner, H. Vogel, Nanoscale **3**(3), 1102 (2011).
[42] Z. Han, X. Yang, X. Shi, L. Wu, P. Hu, H. Fan, F. Teng, Surfaces and Interfaces **54**, 105179 (2024).
[43] J. Li, T. Shi, F. Tian, S. Liu, Q. Fan, Y. Wu, M. Sun, H. Zhang, Y. Lei, F. Liu, S. Zeng, Journal of Catalysis **417**, 1 (2023).
[44] S. Liu, X. Wang, W. Zhao, K. Wang, H. Sang, Z. He, Journal of Alloys and Compounds **568**, 84 (2013).
[45] Q. Simon, D. Barreca, A. Gasparotto, C. Maccato, T. Montini, V. Gombac, P. Fornasiero, O. I. Lebedev, S. Turner, G. Van Tendeloo, Journal of Materials Chemistry **22**(23), 11739 (2012).
[46] M. Deng, Z. Li, S. Liu, X. Fang, L. Wu, Nature Communications **15**(1), 8789 (2024).
[47] A. U. Ubale, Y. S. Sakhare, S. M. Bombatkar, Materials Research Bulletin **48**(9), 3564 (2013).
[48] A. Kathalingam, D. Vikraman, H. S. Kim, H. J. Park, Optical Materials **66**, 122 (2017).
[49] J. Ma, K. Wang, L. Li, T. Zhang, Y. Kong, S. Komarneni, Ceramics International **41**(2), 2050 (2015).
[50] S. Siol, J. C. Hellmann, S. D. Tilley, M. Graetzel, J. Morasch, J. Deuermeier, W. Jaegermann, A. Klein, ACS Applied Materials & Interfaces **8**(33), 21824 (2016).
[51] M. Yang, L. Zhu, Y. Li, L. Cao, Y. Guo, Journal of Alloys and Compounds **578**, 143 (2013).
[52] A. Shukla, V. K. Kaushik, D. Prasher, Electronic Materials Letters **10**, 61 (2014).
[53] L. Shooshtari, R. Mohammadpour, ECS Journal of Solid State Science and Technology **7**(2), P60. (2018).
[54] Z. He, Y. Xia, B. Tang, X. Jiang, J. Su, Materials Letters **184**, 148 (2016).
[55] H. Zhu, C. X. Shan, L. K. Wang, J. Zheng, J. Y. Zhang, B. Yao, D. Z. Shen, The Journal of Physical Chemistry C **114**(15), 7169 (2010).
[56] Y. Hu, X. Zhang, X. Mo, J. Chu, X. Fang, Z. Li, Advanced Functional Materials **35**(8), 2412015 (2025).
[57] E. Hong, Z. Li, X. Zhang, X. Fan, X. Fang, Advanced Materials **36**(29), 2400365 (2024).
[58] Y. Chen, C. H. Chuang, Z. Qin, S. Shen, T. Doane, C. Burda, Nanotechnology **28**(8), 084002 (2017).
[59] Y. Z. Chen, S. W. Wang, T. Y. Su, S. H. Lee, C. W. Chen, C. H. Yang, K. Wang, H. C. Kuo, Y. L. Chueh, Small **14**(22), 1704052 (2018).
[60] N. Kaur, A. Ghosh, P. Bisht, A. Kumar, V. Kaushik, N. Kodan, R. Singh, B. R. Mehta, Journal of Materials Chemistry C **10**(38), 14220 (2022).
[61] R. Kumar, D. Das, A. K. Singh, Journal of Catalysis **359**, 143 (2018).
[62] H. Li, H. Alradhi, Z. Jin, E. A. Anyebe, A. M. Sanchez, W. M. Linhart, R. Kudrawiec, H. Fang, Z. Wang, W. Hu, Q. Zhuang, Advanced Functional Materials **28**(8), 1705382 (2018).
[63] J. Xiao, L. Zhang, H. Zhou, Z. Shao, J. Liu, Y. Zhao, Y. Li, X. Liu, H. Xie, Y. Gao, J. T. Sun, A. T. S. Wee, H. Huang, ACS Applied Materials & Interfaces **12**(28), 32099 (2020).

*Corresponding author: zhuyue199634@163.com